Advances in Concrete Construction, *Vol. 10, No. 1 (2020) 71-79*
DOI: https://doi.org/10.12989/acc.2020.10.1.071

Investigation of flexural behavior of a prestressed girder for bridges using nonproprietary UHPC

Hoa D. Pham[1a], Tung Khuc*[1], Tuan V. Nguyen[2b], Hung V. Cu[1c], Danh B. Le[1d] and Thanh P. Trinh[1e]

[1]Department of Bridges and Highways Engineering, National University of Civil Engineering, Vietnam
[2]Department of Building Materials, National University of Civil Engineering 55 Giai Phong road, Hai Ba Trung district, Hanoi, Vietnam

(*Received March 10, 2020, Revised June 10, 2020, Accepted July 2, 2020*)

Abstract. Ultra-high-performance concrete (UHPC) is recognized as a promising material in future civil engineering projects due to its outstanding mechanical and durability properties. However, the lack of local UHPC materials and official standards, especially for prestressed UHPC structures, has limited the application of UHPC. In this research, a large-scale prestressed bridge girder composed of nonproprietary UHPC is produced and investigated. This work has two objectives to develop the mixing procedure required to create UHPC in large batches and to study the flexural behavior of the prestressed girder. The results demonstrate that a sizeable batch of UHPC can be produced by using a conventional concrete mixing system at any precast factory. In addition, incorporating local aggregates and using conventional mixing systems enables regional widespread use. The flexural behavior of a girder made by this UHPC is investigated including flexural strength, cracking pattern and development, load-deflection curve, and strain and neutral axis behaviors through a comprehensive bending test. The experimental data is similar to the theoretical results from analytical methods based on several standards and recommendations of UHPC design.

Keywords: local UHPC; prestressed girder; flexural behavior; large-scale testing; bridge

1. Introduction

Ultra-high-performance concrete (UHPC) is a sustainable concrete class featuring outstanding mechanical and durability characteristics. Although there are several definitions related to UHPC strength, the lowest compressive strength is usually 120 MPa, while the tensile strength is greater than 8 MPa (Graybeal 2011). Due to its advanced properties, UHPC is a promising replacement for conventional materials in various applications, especially in bridge engineering (Binard 2017, Zhou *et al*. 2018). Since many existing bridges exhibit aging deterioration and damage after being in service for extended periods, using more durable materials is of interest to by many owners such that the budget for inspection and maintenance can be minimized. Moreover, by using UHPC material, bridge structures can be designed, thus reaching a new high limit of span length while simultaneously reducing structural cross-section sizes. The advantages of using UHPC have paved new approaches in several bridge engineering implementations, including in bridge design, accelerated bridge construction, bridge maintenance, and retrofitting.

Perceiving potential of this new class of concrete, numerous studies related to UHPC behavior were carried out over the last two decades reviewed by several researchers (Yoo and Yoon 2016, Zhu *et al*. 2020). Although much UHPC research is introduced, there are a few studies focusing on prestressed beams, which are the most important components in bridges. A prominent expert, Graybeal, conducted a bending test of a full-scale prestressed UHPC girder (24 m long) in 2008 to investigate flexural behavior (Graybeal 2008), which continues to be one of the most comprehensive experiments conducted on a UHPC beam. The Graybeal's study found out some advantages of using UHPC for prestressed girders including higher flexural capacities and smaller width cracks due to fiber reinforcement. The performance of tensile softening due to steel fibers in UHPC was studied in an experimental research on four prestressed UHPC T-beams (5 m long) in 2011, which allowed more precise prediction of flexural strength (Yang *et al*. 2011). The main contribution of that study is to propose an analytical procedure for calculating flexural strength. Another research group redesigned and tested several small-scale prestressed UHPC beams (4.9 to 7.6 m) to explore the structural behavior for different types of cross sections (Giesler *et al*. 2018, Manning *et al*. 2016). Based on these analyses, it was confirmed that the UHPC

*Corresponding author, Ph.D.
E-mail: tungkd@nuce.edu.vn
[a]Associate Professor
E-mail: phamduyhoa@nuce.edu.vn
[b]Ph.D.
E-mail: tuannv@nuce.edu.vn
[c]Ph.D.
E-mail: hungcv@nuce.edu.vn
[d]Ph.D.
E-mail: danhlb@nuce.edu.vn
[e]Research assistant
E-mail: thanhtp@nuce.edu.vn

http://www.techno-press.org/?journal=acc&subpage=7
ISSN: 2287-5301 (Print), 2287-531X (Online)

girder with a smaller cross section outperformed the girder made by conventional concrete. Furthermore, the measured moment was usually higher than the designed moment capacity determined by using the load and resistance factor design specifications of the American Association of State Highway and Transportation (AASHTO LRFD); at times, it was up to 1.58 times higher. Procedures for designing UHPC girders have also been proposed in several bridge projects delivering advantages such as reducing the sizes of cross sections, decreasing the number of girders, and cutting down the amount of reinforcement bars (Almansour and Lounis 2010, Taylor *et al*. 2013). Finite element models of prestressed UHPC girders have also been developed to optimize the relationship of cross-section size versus span length to enhance cost effectiveness since UHPC is so expensive (Zhang and Graybeal 2014). Moreover, flexural capacities calculated by different approaches including AASHTO LRFD, the French interim recommendations (AFGC), the recommendation of the Japan society of civil engineers for the design and construction of UHPC structures (JSCE), and the Canadian highway bridge design code (CSA), were compared to obtain the most suitable design scheme for reinforced and prestressed UHPC structures (Almansour and Lounis 2010, Shafieifar *et al*. 2018, Steinberg 2009).

Along with conducting research and experiments in laboratories, UHPC has been applied in real bridges in pilot projects in several countries. The Sherbrooke pedestrian bridge in Canada (1997) was the first bridge in the world to be built using UHPC, which consists of two 60-m trusses made of UHPC-confined tubes carrying a UHPC slab (Blais and Couture 1999). Subsequently, a series of pilot UHPC bridges were built in other countries, for example, the Bourge-lès-Valence bridge in France (2001) (Hajar *et al*. 2004), the Sakata-Mirai bridge in Japan (2002) (Tanaka *et al*. 2002), the Seonyudo bridge in Korea (2002) (Behloul and Lee 2003), the Mars Hill bridge in the United States (2006) (Wipf *et al*. 2009), and the Friedberg bridge in Germany (2007) (Knippers *et al*. 2010). The Bourge-lès-Valence bridge was the first UHPC bridge to be constructed on highways. Thereafter, UHPC material was used in other bridge projects, as listed in the Russell and Graybeal report (Russell *et al*. 2013). Recently, UHPC bridges were vastly constructed in Malaysia by capitalizing on cost effective local materials, thus enabling the possible for an industrial use of UHPC in bridge construction in that country (Voo *et al*. 2014). It is worth noting that the bridge girders of the pilot UHPC bridges were usually designed and analyzed on a case-by-case basis, considering normal bridge design specifications such as CSA, AASHTO LRFD, or a combination thereof with initial recommendations for reinforced UHPC components (for example, AFGC and JSCE). Moreover, many pilot UHPC bridges were the outcomes from corresponding research, in which numerous experiments were conducted to confirm the reliability of prestressed UHPC girders. Recently, France became the first country to introduce a national standard for designing UHPC structures (NF P18-710); however, detailed specifications for calculating prestressed bridge structures have not been included yet.

Currently, hundreds of UHPC bridge projects are found throughout the world. However, the number of projects utilizing UHPC for the main bridge girders is still limited, especially compared to the total number of new bridges being constructed every year. There are two main reasons explaining its limited application, which include 1) the lack of local UHPC materials, and 2) the inadequacy of standards and recommendations for designing prestressed UHPC girders for bridges. The literature review also reveals that UHPC properties vary due to regional admixtures, mixing processes and facilities as well as concreting methods (Giesler *et al*. 2016). The changes may sequentially affect the mechanical properties of UHPC girders; this requires further investigation locally. Motivated by such challenges, the objectives of this study are 1) to introduce a UHPC mixture using local materials and mixed by a conventional concrete mixer, and 2) to experimentally investigate the behavior of a large-size prestressed girder fabricated with the same UHPC. The main structural behavior studied herein is flexural strength analyzed through a bending test. The outcomes of this research will provide useful information and knowledge for constructing a pilot bridge on road using local UHPC in Vietnam.

2. Local UHPC: Aggregates, mixing procedure and properties

2.1 Mixture proportions using local materials

UHPC is considered to be a breakthrough material technology among other new materials developed for use in civil engineering. It is because of its superior mechanical characteristics including very high compressive strength and elastic modulus, good tensile strength and post-cracking tensile capacity, and great impact resistance. Moreover, UHPC exhibits low permeability yielding excellent durability against severe environments. These remarkable properties are achieved due to several basic principles such as the elimination of coarse aggregates for homogeneity, optimization of the granular mixture, minimization of mixing water for compacted density, and incorporation of small-sized steel fibers for ductility. In Vietnam, UHPC was initially studied and produced at laboratory scales starting in 2012 by using local aggregates except for silica fume (SF) and superplasticizer (SP) (Nguyen *et al*. 2012). The study concluded that Vietnamese Portland cement and fine quartz sand were found to be completely suitable for UHPC. It should be noted that quartz sand, counting the highest ratio of the total material content, is inexpensive in Vietnam due to its ubiquitous nature. In that study, several mixture proportions of UHPC were developed for designing compressive strength ranging from 120 to 150 MPa. Recently, new mixtures have been studied and successfully tested to partially replace SF by other types of mineral admixtures such as fly ash from thermal power plants or ground granulated blast-furnace slag (GGBFS) from steel and iron factories, thus the cost of UHPC is further reduced and a solution is offered in waste management (Nguyen *et al*. 2013).

Table 1 The UHPC mixture composition

Material per 1 m^3 UHPC						
Steel fiber (kg)	Quartz sand (kg)	Cement (kg)	SF (kg)	GGBFS (kg)	SP (kg)	Water (kg)
158	1100	770	110	220	8.25	176

Table 2 Chemical compositions of cement PC40, SF and GGBFS

Materials	Chemical composition (%)								
	SiO_2	Fe_2O_3	Al_2O_3	CaO	MgO	Na_2O	K_2O	SO_3	Ti_2O
Cement	20.3	5.05	3.51	62.81	3.02	-	-	2	-
SF	92.3	1.91	0.86	0.32	0.85	0.38	1.22	0.3	-
GGBFS	34.52	0.66	12.38	41.54	7.25	0.43	0.24	-	-

Fig. 1 The industrial concrete mixer and the facilities of the local precast plant

In this work, the mixing composition is meant for use in a pilot bridge project. Thus, the UHPC design is conservatively selected for design compressive strength of 120 MPa. The UHPC aggregates consist of regional ground quartz sand with a mean particle size of 300 μm, Portland cement PC40 with a mean particle size of 11.4 μm, GGBFS with a mean particle size of 7.2 μm, and SF with a mean particle size of 0.15 μm that was recently produced in Vietnam. Replacement of a large portion of the SF by GGBFS, which is 10 times cheaper than SF (unit weight price), has decreased the price of local UHPC. The steel fiber exhibits a straight profile with a diameter of 0.2 mm and a length of 13 mm; its tensile strength is 2750 MPa according to the material datasheet. The amount of fiber is fixed at 2% by volume of concrete. The SP is a polycarboxylate-based powder that is dry premixed with other aggregates and subsequently packed in 50-kg small bags or 500-kg batches. Considering the proportion of polycarboxylate superplasticizer powder is 0.75% by weight. The water-cementitious material (i.e., cement PC40, GGBFS, and SF) ratio designed for the mixture is 0.16 by weight. Details of the proposed UHPC mixture proportions are summarized in Table 1, and the chemical compositions of the main local materials such as cement PC40, GGBFS, and SF are shown in Table 2.

2.2 Mixing procedure and properties of local UHPC

In this research, a large batch of UHPC is required due to the size of the experimental girder (about 0.4 m^3). Moreover, studying to produce large batches of UHPC is essential for constructing a pilot UHPC bridge later. Due to the intended application of the UHPC, the mixing procedure was developed in collaboration with a local precast factory

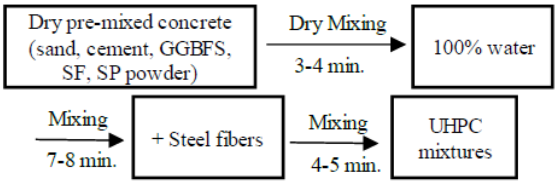

Fig. 2 The mixing procedure using an industrial 1-m^3 concrete mixer

Fig. 3 Specimen tests for obtaining UHPC properties

Table 3 UHPC mechanical properties from specimen tests

Material characteristics	Average (Min – Max)
Compressive strength – ASTM C39M 28-days	120.3 (110.8 – 132.2) MPa
Compressive strength – ASTM C39M 3-days	98.2 (93.1 – 104.8) MPa
Modulus of elasticity – ASTM C469M 28-days	41.1 (38.2 – 46.9) GPa
Modulus of elasticity – Estimated from compressive strength (Graybeal equation)	42.1 (40.4 – 44.1) GPa
Tensile cracking strength – ASTM C1609M; 28-days	8.1 (6.8 – 9.4) MPa
Poisson ratio – ASTM C469M 28-day ratio	0.209 (0.165 – 0.249)

by using their industrial 1-m^3 concrete mixer (Fig. 1). This process was initially studied in the laboratory with a small mixer; and subsequently established after producing two trial batches of 0.3 and 0.7 m^3 with the 1-m^3 concrete mixer. A flow chart of the mixing procedure including time durations for each step is presented in Fig. 2. It is recommended that a new mixing process must be studied according to the mixer being used.

The UHPC mixture produced by local materials and a conventional concrete mixer was tested for obtaining its characteristics. In this study, compressive strength f_c' is determined from 9 cylinders of 100 mm diameter and 200 mm height according to ASTM C39M. The modulus of elasticity E_c and Poisson ratio ρ are estimated following ASTM C469M on the same cylinder samples of the compressive tests. The tensile cracking strength f_t is obtained from 9 prisms of 400-mm long having a cross-section size of 100 mm×100 mm (ASTM C1609M). In each cylinder specimen, three strain gauges including two vertical gauges and one horizontal gauge were adhered to simultaneously measure the vertical strain for calculating the modulus of elasticity E_c, and the hoop strain for determining the Poisson ratio ρ. Because prestressing strands were released on the 3rd day of age of the prestressed UHPC girder, compressive strength was

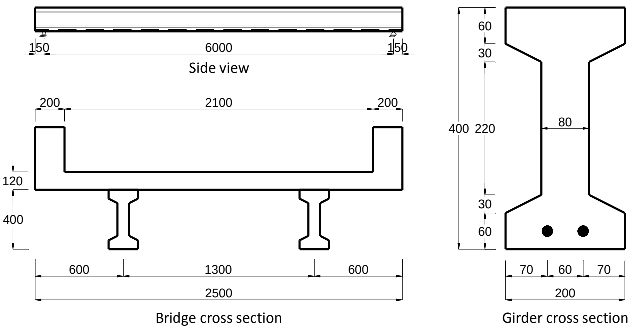

Fig. 4 The pedestrian bridge and I-girder cross section. Dimensions are given in millimeter

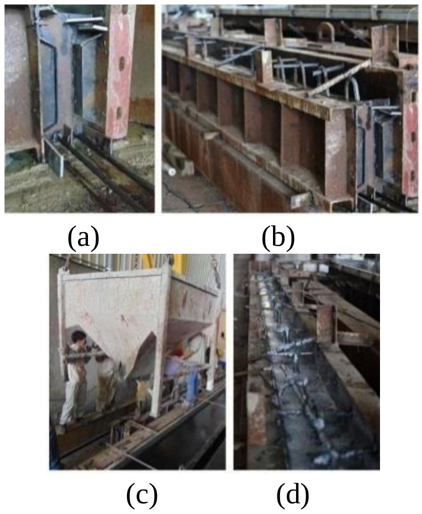

Fig. 5 The I-girder fabrication procedure including (a) Prestressing strands, (b) Preparing steel formwork, (c) Casting UHPC, (d) Curing of UHPC

additionally determined at the 3rd day of age of other 9 UHPC cylinders. All specimen setting tests are demonstrated in Fig. 3. The modulus of elasticity E_c was also estimated by another method from compressive strength f_c' based on Eq. (1) proposed by Graybeal (2007).

$$E_c = 3840\sqrt{f_c'} \qquad (1)$$

The properties of the local UHPC measured from specimen testing are listed in Table 3. The mechanical properties of the UHPC produced by the industrial 1-m^3 concrete mixer are very close to the design values. Therefore, the results initially confirm that the proposed mixing process can produce good UHPC mixture quality that agrees with the design requirement.

3. Experiment

3.1 Girder design and fabrication

Although the girder is precast for the experimental aim in this study, it is designed as a girder of a pedestrian bridge with a supported span of 6 m. The bridge consists of two prestressed UHPC I-girders, each 6.3-m long and composited to a normal concrete deck (12-cm thick). The design procedure corresponds to the AASHTO LRFD 2012 (AASHTO 2012) specifications with modifications of the UHPC mechanical properties. Because the fibers in UHPC can contribute significantly to shear capacity (Wang *et al*. 2019), the girder is designed without mild steel reinforcement, which was recommended in earlier studies (Giesler *et al*. 2018, Manning *et al*. 2016, Voo *et al*. 2014).

Fig. 4 presents a drawing of the designed UHPC girder. The depth of the girder is 400 mm while the web thickness is 80 mm due to there being no stirrups. The bulb dimensions are determined based on AASHTO LRFD 2012 of clear cover over strands, distances between strands, and engineer recommendations for girder fabrication and construction. A total of two 15.2-mm prestressing strands is placed 30 mm from the bottom face of the girder (placement decided according to verifying calculations). The chosen strands are grade 1860 low-relaxation with an ultimate strength of 1860 MPa and an elastic modulus of 200 GPa, according to material datasheets. The strands are jacked to 75% of their ultimate strength.

The prestressed UHPC I-girder is fabricated in the regional precast concrete factory as illustrated in Fig. 5. It is cast with only a single UHPC mixture batch of 0.5 m^3, which is mixed by a conventional blender through the proposed procedure (Fig. 2). The formwork system is fabricated from steel plates. Due to the high workability of the UHPC mixture, edges between formwork components require filling by hot-melt adhesive and duct tape to reject UHPC grout leakage. The UHPC mixture is poured from one end to the other end of the girder to ensure that the steel fibers have a proper orientation (parallel to the flow of the UHPC mixture). Although the time for mixing UHPC is longer than the mixing time required for conventional concrete, the casting time of UHPC is quite fast due to its workability. The UHPC placement time of this I-girder is timed at less than 15 minutes. The formwork is released the next day, and the strands are cut and transferring prestressing load on the 3rd day of age when the average compressive strength of 98.2 MPa is higher than 72 MPa (corresponding to 60% of design f_c'). Since the strands are jacked up to 75% of their ultimate strength, a compressive force to the girder is approximately 390 kN. The girder calculation sheets show that the total release loss is about 90 MPa (corresponding to 6.5% of the jacking stress), and the total final loss is approximately 322 MPa (corresponding to 23.1% of the jacking stress).

3.2 Test setup and instrumentation

The girder is investigated by using a four-point flexural simple beam test. Following this setup, the testing load is applied to the girder on two points that are symmetrically located 0.5 m from the midspan. The testing load is induced by a jack and then distributed to two points through a steel spreader beam (Fig. 6). During the loading test, the load level is decreased two times to the initial state to observe the residual stiffness of the girder. As the girder length is 6.3 m, it is placed on two pinned supports located 6 m from each other. This structural layout provides a constant

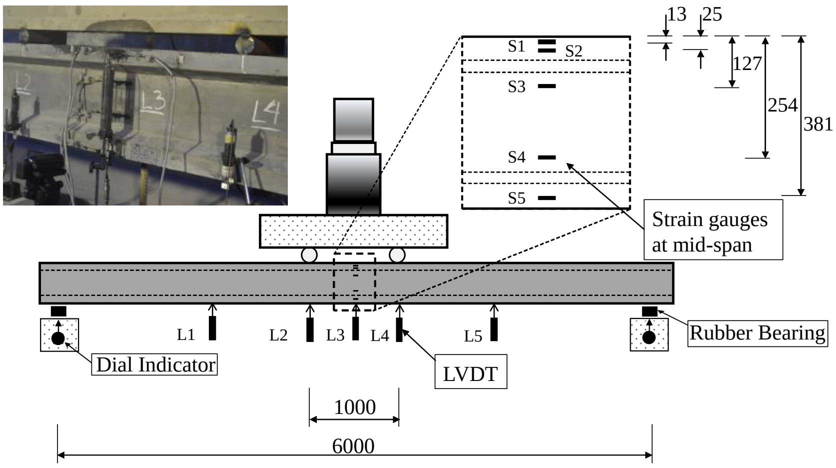

Fig. 6 Experimental setup and instrumentation of the I-girder testing. Dimensions are given in millimeter

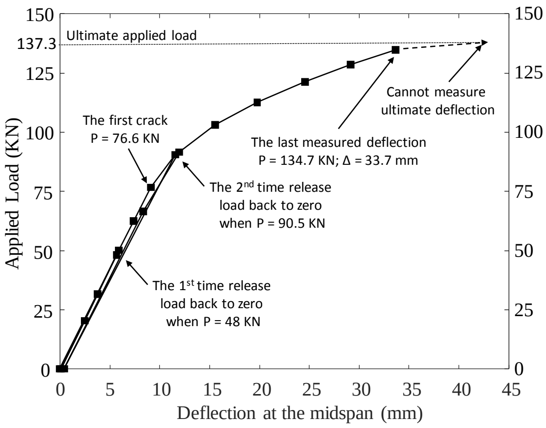

Fig. 7 Load versus deflection in the midspan of the I-girder

maximum moment region of 1 m (distance between two loading points).

The girder is instrumented with numerous sensors including five strain gauges, five linear variable differential transformers (LVDTs), and two mechanical dial indicators. To observe the strain profile and the neutral axis (NA) location of the maximum moment section during the experiment, all strain gauges are bonded on the side of the midspan section at 13, 25, 127, 254, and 381 mm down from the top extreme fiber. Displacements of the girder are measured by means of five LVDTs that are installed at the midspan, at two loading points, and at two other quarter-span points. Due to the use of rubber supports, two mechanical dial indicators are set up for obtaining bearing settlements. All sensors are connected to a data acquisition system exception of two mechanical dial indicators, which are visually read after each loading level. A diagram of the instrumentation system is illustrated in Fig. 6.

4. Results and discussion

4.1 Load – Deflection behavior

Deflections of the girders are captured at every loading step including increasing and decreasing levels through five LVDTs. These datasets are used to develop the load vs. deflection curve at the midspan that is shown in Fig. 7. Following the loading plan, the load is increased up to 48 kN, and it is subsequently decreased to the initial stage. When releasing the induced load back to zero, the deflections of the girder measured from all LVDTs return to approximately zero. This observation demonstrates that during the loading phase from 0 to 48 kN, the girder is still working on its elastic behavior. The first crack is detected by observation and a slight cracking sound directly after loading at 76.6 kN. This behavior is also confirmed later from the load-deflection curve since the curve starts to soften after that datapoint, indicating a sign of inelastic behavior. Although the beginning of the inelastic stage is around 76.6 kN of the applied load, the girder can further carry an additional load that subsequently reaches the ultimate value of 137.3 kN, which is 179% higher than the first cracking load. The maximum acquired deflection at the midspan is 33.7 mm corresponding to the applied load of 134.7 kN. Unfortunately, the ultimate deflection at the midspan (corresponding to the ultimate load of 137.3 kN) cannot be determined due to the midspan LVDT being out of range in that scenario.

In this bending test, the relationship between the applied load and deflection at the elastic stage is used to determine the modulus of elasticity E_c of the UHPC. The E_c values are also compared to those obtained from the specimen tests presented in Table 3. Generally, E_c can be determined from the relationship between the applied load and deflection at the elastic stage based on Castigliano's theorem, as given in Eq. (2).

$$E_c = \int \frac{Mm}{I\Delta} dx \tag{2}$$

where E_c is the modulus of elasticity of the girder material (GPa), M is the bending moment due to the applied load (MPa), m is the bending moment at the measurement deflection location due to the unit load, I is the moment of inertia (m^4), and Δ is the deflection at the measurement position (m).

Table 4 shows the modulus of elasticity determined by using measurement deflections from all LVDTs. Because

Table 4 Elastic modulus determined from the load-deflection behaviour

Load (kN)	E determined from LVDT1 (MPa)	E determined from LVDT2 (MPa)	E determined from LVDT3 (MPa)	E determined from LVDT4 (MPa)	E determined from LVDT5 (MPa)
48.0	43,408	39,295	39,327	38,827	38,872
31.5	42,899	38,283	38,353	38,353	38,325
50.1	43,136	39,281	39,354	38,942	39,106
62.4	42,649	39,393	39,202	38,765	38,863
Mean values	43,023	39,063	39,059	38,722	38,792

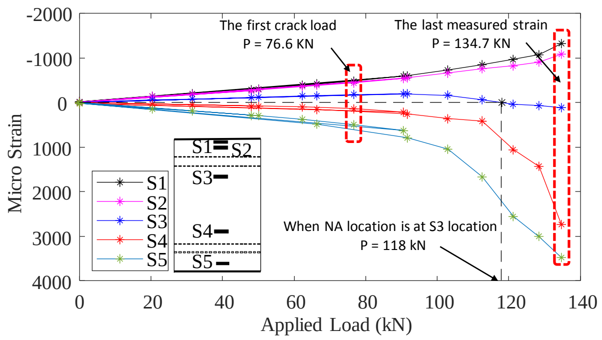

Fig. 8 The strain behavior at the midspan section of the I-girder

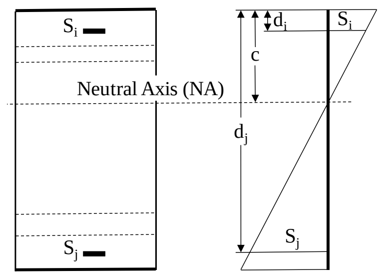

Fig. 9 The theory of planar strain distribution

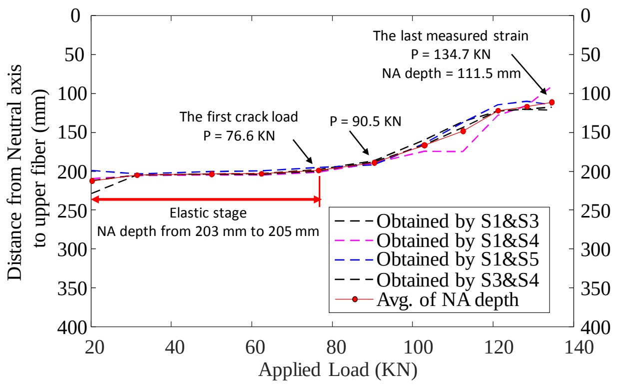

Fig. 10 The neutral axis (*NA*) depth during I-girder test

Eq. (2) is derived for a girder working elastically, measurement deflections used for E_c determination are selected corresponding to the loads less than 76.6 kN (the first cracking load). The average E_c value of UHPC obtained by this approach is 39.7 GPa, which is barely less than the value measured by the specimen tests in Table 3 (41.1 GPa). This difference is about 3.4% and is considered reasonable, as it can be caused by measurement uncertainties.

4.2 Strain behaviour and Neutral Axis (NA) locations

There is a total of five strain gauges placed at the midspan section from the top to the bottom fibers. Fig. 8 illustrates the strain values acquired from all sensors during the experiment until the last measured values corresponding to the applied load of 134.7 kN. Fibers corresponding to the strain gauge *S*1 and *S*2 are always compressed. On the other hand, the opposite is observed for the fibers of *S*4 and *S*5. It is interesting to note that the strain values obtained by *S*3 change from compressive to tensile when the loading level is increased. This observation may be caused by the NA locations of the girder rising due to cracking developing from the bottom of the girder. The curve of gauge *S*3 also illustrates that the location of *NA* is exactly at the location of gauge *S*3 (approximately 127 mm from the top fiber) when the applied load is 118 kN (Fig. 8). The maximum compressive strain value is recorded at 0.00133 by the top gauge *S*1, which is much lower than the ultimate strain of approximately 0.0035 determined by the specimen tests.

The strain values are also used to determine the NA locations of the girder. Based on strain values S_i and S_j of two gauges attached at two fibers *i* and *j*, the NA depth from the top of the girder is calculated as given in Eq. (3).

This equation can be easily derived based on the assumption of the girder section remaining planar under any load scenario, as illustrated in Fig. 9.

$$c = \frac{S_i d_j - S_j d_i}{S_i - S_j} \tag{3}$$

where d_i is the distance from the top fiber to the fiber *i*, and d_j is the distance from the top fiber to the fiber *j*.

Fig. 10 shows the *NA* depth versus the applied load calculated by strain datasets from several pairs of gauges including *S*1 & *S*3, *S*1 & *S*4, *S*1 & *S*5 and *S*3 & *S*4. It is seen that four *NA* depth graphs determined using 4 pairs of gauges are analogous. Therefore, the average *NA* depth graph (red line) is represented for the final *NA* depth data versus the applied load of the experimental girder. The average *NA* depth graph additionally confirms that an inelastic stage occurs after the first crack load of 76.6 kN. Fig. 10 also indicates that the *NA* positions of the girder are rather stable between 203 and 205-mm depth in the elastic stage, which are compared to the theoretical value of 203.6 mm. However, they quickly rise after the girder shifted to inelasticity. At the applied load of 134.7 kN, the depth of the *NA* from the top fiber is determined to be approximately 111.5 mm.

4.3 Cracking behaviors and failure mode

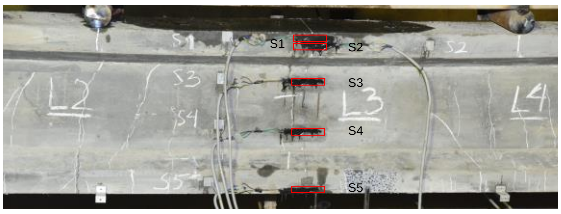

Fig. 11 Typical crack pattern on the pure bending area of I-girder

Fig. 12 The rupture failure mode of I-girder

Cracking behavior is checked periodically after each loading level in order to detect the first crack and to monitor crack propagation and development. The first micro-crack is identified at the loading level of 76.6 kN by a minor cracking pitch and by subsequent visual confirmation. The first crack is on the bottom surface between the two loading points, which is a pure bending region of the girder. New cracks appear for loading levels beyond the current ones; most cracks are found in the pure bending area (Fig. 11). In addition, the cracks do not obviously widen upon increased loading. The observation indicates that the stress induced by additional loading have been redistributed, thus creating new cracks due to the better homogeneous nature of UHPC comparing to normal concrete, which may be formed by the fibers bridging reinforcement and fine aggregates. This cracking observation is very different from the cracking behavior of conventional concrete, which may provide insight into why UHPC girders exhibit prolonged usage after the first crack occurs.

The failure of the experimental girder is rupture mode because two prestressed strands are ruptured before the UHPC on the top fiber of girder is crushed (Fig. 12). In this experiment, the failure mode can be initially explained by considering that the steel fibers may prevent cracking development upward and keep the *NA* depth lower. It is worth noting that this failure is an unexpected mode for beam structures, thus investigation of the minimum number of strands should be a subject for prestressed UHPC girder design.

5. Flexural strength analysis

5.1 Flexural resistance based on an inversed method

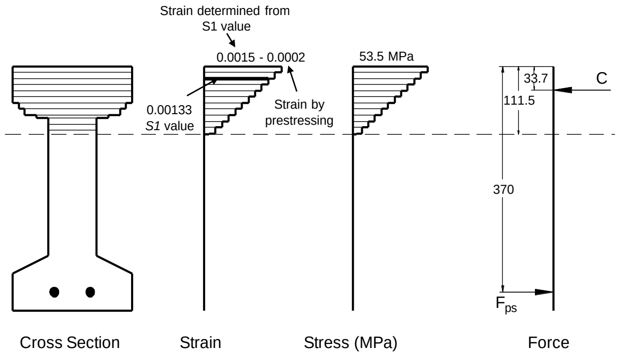

Fig. 13 Multiple layer modeling for determining flexural resistance

In this section, the flexural strength of the girder is determined by the inversed method based on measured strain data and observation of the failure mode. The absolute compressive strain of the top fiber is calculated only 0.0013 based on the *S*1 strain value, the tensile strain due to prestressing, and the final *NA* depth of 111.5 mm. Since the top fiber strain (0.0013) is much less than the ultimate strain of UHPC (0.0035), the stress distribution of the compressive zone is assumed elastically linear from zero at the final *NA* location of 111.5 mm. To determine the location of the compressive load, the compressive zone is divided into multiple layers over its height, as shown in Fig. 13. The distance d_c from the top fiber to the compressive load location is 33.7 mm, which can be used to determine the predicted flexural capacity of the girder as Eq. (4) with considering the exclusion of UHPC tension behavior.

$$M = A_s f_{ps}\left(d_p - d_c\right) = 180.6\ KNm \qquad (4)$$

where f_{ps} is stress in prestressing steel at the time for which the flexural resistance of the girder is required. In this test, f_{ps} is 1860 MPa due to rupture of strands. A_s is the total area of the strands, d_p is the distance from the centroid of strands to the top fiber. Since the total bending moment induced by the ultimate applied loading and the girder self-weight is 177.2 kNm, this effect is highly similar to the predicted flexural capacity of the girder calculated by Eq. (4). The difference between the two values (about 1.9%) is further confirmation of the flexural behavior and failure mode described in previous section.

5.2 Flexural resistance based on standards

In this study, a new standard of NF P18-710 France Standard (AFNOR 2016) and the report of Federal Highway Administration (FHWA) (Graybeal 2006) are used to determine the girder's flexural capacity. It should be noted that both approaches include the tensile behavior of the UHPC when determining the flexural strength. Although the stress-strain graphs of UHPC are different between two methods, predicting the flexural capacity of a girder follows Euler-Bernoulli beam theory. This theory assumes that at the failure state, the girder section remains planar, and equilibrium of internal and external forces is legitimate. Subsequently, the flexural capacity is determined by

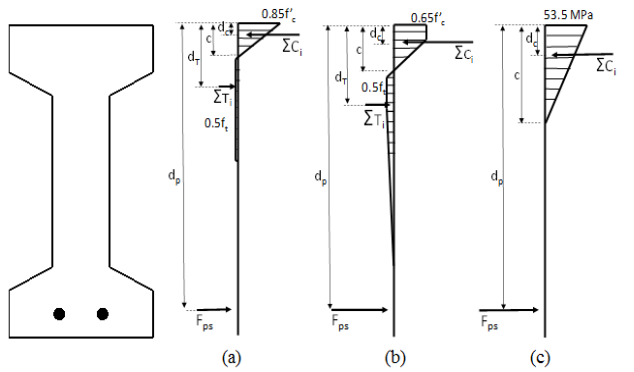
Fig. 14 Stress distribution throughout girder cross-section determined based on (a) FHWA 2006, (b) NF18-710, (c) Inversed method

assuming strain at the most compressive fiber approaching the allowable compressive strain while the stress in prestressing strands reaches f_{ps}. Generally, determining the flexural capacity of a UHPC girder is implemented as follows. First, the stress distribution over the height of the girder is determined based on the stress-strain behavior of UHPC according to a selected standard or recommendation. Then, an equilibrium force equation is developed to estimate the NA position at the failure state. Finally, the flexural capacity of the girder is calculated by Eq. (5).

$$M = \sum C.(c - d_C) + \sum T.(d_T - c) + A_s f_{ps}(d_p - c) \quad (5)$$

where T is the tensile load of the UHPC tension zone, d_T is the distance from the tensile load to the top fiber, C is the compressive load of the UHPC compression zone, d_C is the distance from the compressive load to the top fiber, and c is the *NA* depth. In this equation, f_{ps}, the stress in the prestressing steel at the failure state (please refer AASHTO LRFD (AASHTO 2012)), is the same as that in the conventional prestressed concrete analysis, which is detailed in Eq. (6).

$$f_{ps} = f_{pu}(1 - k\frac{c}{d_p}) \quad (6)$$

in which

$$k = 2(1.04 - \frac{f_{py}}{f_{pu}}) \quad (7)$$

where f_{pu} is the ultimate tensile strength of prestressed strands and f_{py} is the yield strength.

Fig. 14 illustrates the stress distributions throughout the girder depth as calculated following FHWA 2006, NF P18-710 recommendations, and the inversed method using measured data. Although the inversed method presented in previous section does not include the tensile zone of UHPC, the methods based on FHWA 2006 and NF P18-710 have included the effectiveness of the tensile properties of UHPC.

After the stress distributions are computed, the *NA* positions are obtained by means of force equilibrium theory. The predicted flexural resistances determined by different methods are highly similar, which are summarized in Table 5. Although the flexural strength calculated based on the inversed method is smaller than those obtained from the FHWA 2006 and NF P18-710 recommendations, the difference is insignificant, thus indicating that the effectiveness of the tensile zone in UHPC is small. The flexural resistance values are also close to the moment induced by the loading effect (177.2 kNm). This observation demonstrates that it is acceptable to use the current recommendations and standards for calculating the flexural capacity of prestressed UHPC girders.

Table 5 Predicted flexural capacities for the I-girder

	FHWA	NF P18-710	Inversed method based on measured data
c (mm)	46.3	56.3	111.5 (calculated from measured strain data)
d_C (mm)	15.4	20.6	33.7
d_T (mm)	70	121.1	0
f_{ps} (kN/mm^2)	1794.8	1780.8	1860
d_p (mm)	370	370	370
M (kNm)	181.2	184.6	180.6
M by loading effect (kNm)	177.2		

6. Conclusions

In this study, an experimental investigation of the flexural behavior for a prestressed UHPC girder is presented. The girder is produced by using local UHPC and a conventional concrete mixer at a regional precast plant. The outcomes of this study contribute critical information and experience for the planned pilot highway bridge in Vietnam subsequently. In short, several conclusions can be pinpointed.

- The local UHPC produced by regional aggregates provides characteristics similar to these of commercial UHPC. By using regional materials, the cost of UHPC becomes more reasonable.
- A mixing procedure for the UHPC mixture can be developed for common conventional concrete mixing systems in the precast industry. These procedures pave the way for implementing UHPC extensively without exclusive mixers.
- The flexural behavior of the prestressed UHPC girder closely agrees with Euler-Bernoulli beam theory, which is confirmed by the flexural capacities (as predicted by using FHWA, NF P18-710, and the inversed method) being similar to the moment induced by the loading effect with differences from 1.9% to 4.0%. Therefore, there is a reliable method to analyze and design structures made with this new material based on current standards and recommendations.

However, it is worth noting that the fibers bridging reinforcement impede cracking development. Therefore, the compressive zone of a girder may not progress up to the limitation strength of UHPC causing strand rupture. This behavior mitigates the effectiveness of using such this advanced material. Therefore, the minimum requirement of prestressing strands for prestressed UHPC girders should be considered in future research.

Acknowledgements

The authors would like to acknowledge the supports from Vietnam Ministry of Education and Training and National University of Civil Engineering under the CTB-2017-01-03 project.

References

Almansour, H. and Lounis, Z. (2010), "Innovative design approach of precast–prestressed girder bridges using ultra high performance concrete", *Can. J. Civil Eng.*, **37**(4), 511-521. https://doi.org/10.1139/L09-169.

Behloul, M. and Lee, K.C. (2003), "Ductal® seonyu footbridge", *Struct. Concrete*, **4**(4), 195-201. https://doi.org/10.1680/stco.2003.4.4.195.

Binard, J.P. (2017), "UHPC: A game-changing material for PCI bridge producers", *PCI J.*, **62**(2), 34-46.

Blais, P.Y. and Couture, M. (1999), "Precast, prestressed pedestrian bridge world's first reactive powder concrete structure", *PCI J.*, **44**(5), 60-71.

Giesler, A.J., Applegate, S.B. and Weldon, B.D. (2016), "Implementing nonproprietary, ultra-high-performance concrete in a precasting plant", *PCI J.*, **61**(6), 68-80.

Giesler, A.J., McGinnis, M.J. and Weldon, B.D. (2018), "Flexural behavior and analysis of prestressed ultra-high-performance concrete beams made from locally available materials", *PCI J.*, **63**(6), 66-80.

Graybeal, B.A. (2006), "Structural behavior of ultra-high performance concrete prestressed i-girders", Report No. FHWA-HRT-06-115, Federal Highway Administration, McLean, VA, USA.

Graybeal, B.A. (2007), "Compressive behavior of ultra-high-performance fiber-reinforced concrete", *ACI Mater. J.*, **104**(2), 146-152.

Graybeal, B.A. (2008), "Flexural behavior of an ultrahigh-performance concrete I-girder", *J. Bridge Eng.*, **13**(6), 602-610. https://doi.org/10.1061/(ASCE)1084-0702(2008)13:6(602).

Graybeal, B.A. (2011), "Ultra-high-performance concrete", Report No. FHWA-HRT-11-038, Federal Highway Administration, McLean, VA, USA.

Hajar, Z., Lecointre, D., Simon, A. and Petitjean, J. (2004), "Design and construction of the world first ultra-high performance concrete road bridges", *Proceedings of the Int. Symp. on UHPC*, Kassel, Germany, September.

Knippers, J., Pelke, E., Gabler, M. and Berger, D. (2010), "Bridges with glass fibre–reinforced polymer decks: the road bridge in Friedberg, Germany", *Struct. Eng. Int.*, **20**(4), 400-404. https://doi.org/10.2749/101686610793557762.

LRFDUS-6 (2012), AASHTO LRFD Bridge Design Specifications, American Association of State Highway and Transportation Officials (AASHTO), Washington, DC, USA.

Manning, M.P., Weldon, B.D., McGinnis, M.J., Jáuregui, D.V. and Newtson, C.M. (2016), "Behavior comparison of prestressed channel girders from high-performance and ultrahigh-performance concrete", *Tran. Res. Rec.*, **2577**(1), 60-68. https://doi.org/10.3141/2577-08.

NF P18-710 (2016), Design of Concrete Structures: Specific Rules for Ultra-High Performance Fiber Reinforced Concrete (UHPFRC), Association Française de Normalisation (AFNOR), Paris, France.

Nguyen, C.T., Nguyen, V.T., Le, T.T., Pham, H.H. and Ye, G. (2013), "Ultra high performance concrete using a combination of Silica Fume and ground granulated blast-furnace slag in Vietnam", *Proceedings of the International Conference on Sustainable Built Environment for Now and the Future*, Hanoi, VietNam, March.

Nguyen, C.T., Pham, H.H. and Nguyen, V.T. (2012), "Research and development of ultra-high-performance concrete using available materials in Vietnam", *J. Constr.*, **12**, 71-74.

Russell, H.G., Graybeal, B.A. and Russell, H.G. (2013), "Ultra-high performance concrete: a state-of-the-art report for the bridge community", Report No. FHWA-HRT-13-060, Federal Highway Administration, McLean, VA, USA.

Shafieifar, M., Farzad, M. and Azizinamini, A. (2018), "A comparison of existing analytical methods to predict the flexural capacity of ultra high performance concrete (UHPC) beams", *Constr. Build. Mater.*, **172**, 10-18. https://doi.org/10.1016/j.conbuildmat.2018.03.229.

Steinberg, E. (2009), "Structural reliability of prestressed UHPC flexure models for bridge girders", *J. Bridge Eng.*, **15**(1), 65-72. https://doi.org/10.1061/(ASCE)BE.1943-5592.0000039.

Tanaka, Y., Musya, H., Ootake, A., Shimoyama, Y. and Kaneko, O. (2002), "Design and construction of Sakata-Mirai footbridge using reactive powder concrete", *Proceedings of the 1st fib Congress*, Osaka, Japan, October.

Taylor, C.W., Weldon, B.D., Jáuregui, D.V. and Newtson, C.M. (2013), "Case studies using ultrahigh-performance concrete for prestressed girder bridge design", *Pract. Period. Struct. Des. Constr.*, **18**(4), 261-267. https://doi.org/10.1061/(ASCE)SC.1943-5576.0000167.

Voo, Y.L., Foster, S.J. and Voo, C.C. (2014), "Ultrahigh-performance concrete segmental bridge technology: Toward sustainable bridge construction", *J. Bridge Eng.*, **20**(8), B5014001. https://doi.org/10.1061/(ASCE)BE.1943-5592.0000704.

Wang, W., Wu, C., Li, J., Liu, Z. and Zhi, X. (2019), "Lateral impact behavior of double-skin steel tubular (DST) members with ultra-high-performance fiber-reinforced concrete (UHPFRC)", *Thin Wall. Struct.*, **144**, 106351. https://doi.org/10.1016/j.tws.2019.106351.

Wipf, T.J., Phares, B.M., Sritharan, S., Degen, B.E. and Giesmann, M.T. (2009), "Design and evaluation of a single-span bridge using ultra-high-performance concrete", Report No. IHRB Project TR-529, Highway Research Board, Iowa, USA.

Yang, I.H., Joh, C. and Kim, B.S. (2011), "Flexural strength of large-scale ultra-high-performance concrete prestressed T-beams", *Can. J. Civil Eng.*, **38**(11), 1185-1195. http://doi.org/10.1139/l11-078.

Yoo, D.Y. and Yoon, Y.S. (2016), "A review on structural behavior, design, and application of ultra-high-performance fiber-reinforced concrete", *Int. J. Concrete Struct. Mater.*, **10**(2), 125-142. https://doi.org/10.1007/s40069-016-0143-x.

Zhang, G. and Graybeal, B.A. (2014), "Development of UHPC pi-girder sections for span length up to 41 m", *J. Bridge Eng.*, **20**(3), 04014068. https://doi.org/10.1061/(ASCE)BE.1943-5592.0000653.

Zhou, M., Lu, W., Song, J. and Lee, G.C. (2018), "Application of ultra-high-performance concrete in bridge engineering", *Constr. Build. Mater.*, **186**, 1256-1267. https://doi.org/10.1016/j.conbuildmat.2018.08.036.

Zhu, Y., Zhang, Y., Hussein, H.H. and Chen, G. (2020), "Flexural strengthening of reinforced concrete beams or slabs using ultra-high performance concrete (UHPC): A state of the art review", *Eng. Struct.*, **205**, 110035. https://doi.org/10.1016/j.engstruct.2019.110035.

JK